

LETTERS

The emergence of geometric order in proliferating metazoan epithelia

Matthew C. Gibson^{1*†}, Ankit B. Patel^{2*}, Radhika Nagpal² & Norbert Perrimon¹

The predominantly hexagonal cell pattern of simple epithelia was noted in the earliest microscopic analyses of animal tissues¹, a topology commonly thought to reflect cell sorting into optimally packed honeycomb arrays². Here we use a discrete Markov model validated by time-lapse microscopy and clonal analysis to demonstrate that the distribution of polygonal cell types in epithelia is not a result of cell packing, but rather a direct mathematical consequence of cell proliferation. On the basis of *in vivo* analysis of mitotic cell junction dynamics in *Drosophila* imaginal discs, we mathematically predict the convergence of epithelial topology to a fixed equilibrium distribution of cellular polygons. This distribution is empirically confirmed in tissue samples from vertebrate, arthropod and cnidarian organisms, suggesting that a similar proliferation-dependent cell pattern underlies pattern formation and morphogenesis throughout the metazoa.

From sponges to humans, the organization of cells into epithelial sheets is an essential feature of animal design. Historically, the characteristic 'cobblestone' topology of monolayer epithelia has been presumed to reflect optimal cell packing. Many biological and non-biological systems do indeed form predictable geometric arrays due to a tendency either to minimize surface energy or maximize space filling. Prominent examples include insect retinal cells, non-proliferating epithelia, honeycombs, compressed soap bubbles, and even coins pushed together on a tabletop^{2–5}. However, in contrast with these systems, proliferating epithelia rarely exhibit a honeycomb pattern (Fig. 1a), more often forming irregular polygon arrays due to the effect of cell division^{6–9}. The wing primordium (imaginal disc) of the fruitfly *Drosophila melanogaster*, for example, is an epithelial sheet that grows from ~20 to ~50,000 cells during approximately 4 days of larval development^{10–12}. At the level of the adhesive septate junctions that bind cells to their neighbours¹³, the wing epithelium is a heterogeneous lattice dominated by hexagons, but also featuring significant numbers of four- to nine-sided cells (Fig. 1b). Although recent progress has been made in understanding rearrangements of epithelial topology during morphogenesis^{14–16}, the mechanisms that determine cell topology in proliferating epithelia remain poorly defined.

To understand the dynamic process that generates the heterogeneous cell pattern in the *Drosophila* wing, time-lapse movies were collected using fluorescent proteins that localize to the septate junction (ATPase- α -GFP and neuroglian-GFP^{17,18}). Consistent with a negligible role for cell rearrangement in the determination of topology, large-scale sorting or migration within the epithelium was not observed (Supplementary Movie 1). The only significant cellular movements occurred during mitosis, as initially polygonal prophase cells rounded up and divided into two daughter polygons (Fig. 1c; see also Supplementary Movies 2 and 3). Despite marked dilation of mitotic cells in prophase-metaphase (Fig. 1d) and the subsequent contraction of the cytokinetic furrow (Fig. 1e),

cell-neighbour relationships were stably maintained throughout the cell cycle, attesting to an elastic capacity of the junctional lattice to conserve topology over time. These results indicate that cells tightly adhere to their immediate neighbours, consistent with the well-established formation of contiguous cell lineage clones in *Drosophila* appendage primordia^{19–21}.

To characterize more precisely how cells form new interfaces after division, we used the FLP-out technique²² to activate stochastically Gal4 transcription factor activity in individual cells, thereby marking single cell lineages with expression of a *UAS-GFP* transgene. Small GFP⁺ cell clones were then scored to determine directly the spatial relationship between post-mitotic siblings (Fig. 1f). At least 94% of mitoses resulted in the apposition of daughters across a common septate junctional interface (type I, Fig. 1g; $n = 250$ clones). These observations indicate that cytokinesis leads to a transient bottle-neck conformation (for example, Fig. 1e) that predictably resolves with abscission into two polygonal cells adjoined by a common side (Fig. 1h).

If epithelial cells adhere to their neighbours and do not re-sort, then cell division should be sufficient to account for the heterogeneous topology of monolayer epithelia, including the predominance of hexagons. To test mathematically this hypothesis, we defined six logical conditions: (1) cells are polygons with a minimum of four sides ($n = 2,172$ wing disc cells); (2) cells do not re-sort (Supplementary Movies 1–3); (3) mitotic siblings retain a common junctional interface (for example, Fig. 1f); (4) cells have asynchronous but roughly uniform cell cycle times¹²; (5) cleavage planes always cut a side rather than a vertex of the mother polygon (inferred from the observation that 4-cell junctions are rare and presumably unstable); and (6) mitotic cleavage orientation randomly distributes existing tricellular junctions to both daughter cells.

Using conditions 1–5, the wing epithelium can be formulated as a two-dimensional planar network (graph). In topological terms, each tricellular junction is a vertex, each cell side is an undirected edge, and each apical cell surface is a polygonal face. Let v_t , e_t and f_t denote the number of vertices, edges and faces after t divisions. If we assume that cells divide at a uniform rate, then the number of faces (cells) will double after each round of division. Thus, $f_t = 2f_{t-1}$. Furthermore, because each cell division results in biogenesis of two vertices and three edges (for example, Fig. 1h), the number of vertices at time t is $v_t = v_{t-1} + 2f_{t-1}$ and the number of edges is $e_t = e_{t-1} + 3f_{t-1}$. Because boundary effects become negligible for large t (Supplementary Data), we can approximate the average number of sides per cell (s) at division t :

$$s_t = 2(e_{t-1} + 3f_{t-1})/2f_{t-1} = (s_{t-1}/2) + 3 \quad (1)$$

This recurrence system is solvable for the state of the epithelial network as a function of the initial network at time $t = 0$:

$$s_t = 6 + 2^{-t}(s_0 - 6) \quad (2)$$

¹Department of Genetics and Howard Hughes Medical Institute, Harvard Medical School, Boston, Massachusetts 02115, USA. ²Division of Engineering and Applied Sciences, Harvard University, Cambridge, Massachusetts 02138, USA. [†]Present address: Stowers Institute for Medical Research, 1000 East 50th Street, Kansas City, Missouri 64110, USA. *These authors contributed equally to this work.

Equation (2) shows that the average number of cell sides exponentially approaches six, consistent with Euler's theorem. This implies that even in epithelia devoid of minimal packing, the system will assume a predominantly hexagonal topology as a consequence of cell

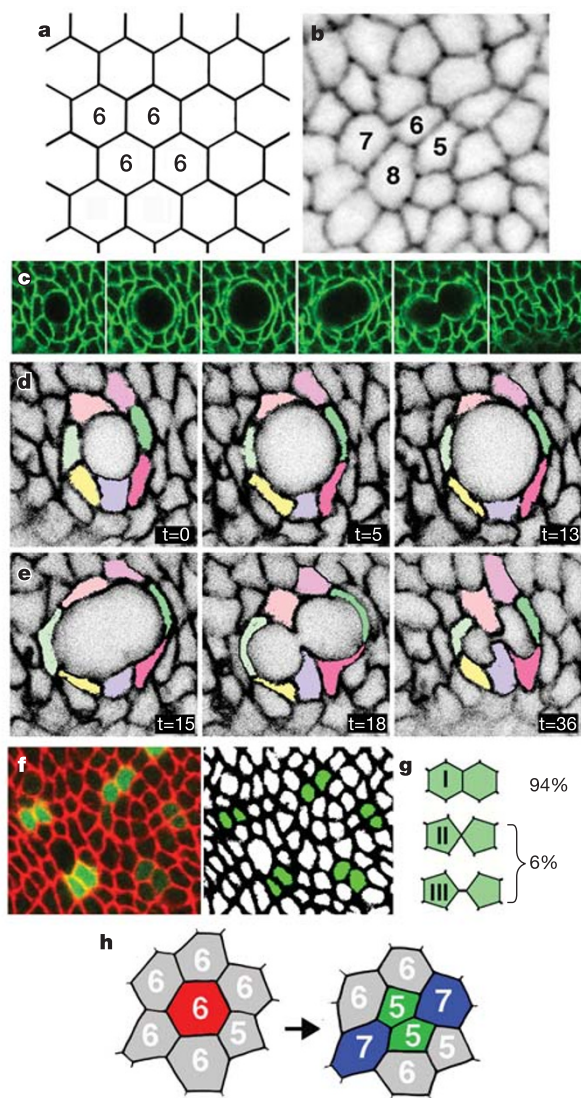


Figure 1 | Mitosis and the *in vivo* dynamics of epithelial topology. **a**, The regular hexagonal array typical of free energy minimization processes is defined by uniformity of cell side length and the formation of tricellular junctions, with each intersecting cell side separated by an equivalent 120° angle. **b**, At the level of the septate junctions (stained here for Discs large (Dlg; black)), cell topology in the wing disc epithelium is highly irregular. **c**, Six successive stages of cell division from a confocal time-lapse recording. Septate junction dynamics, monitored with *nrg*-GFP (green), show that mitotic cells first round up and then divide at the apical epithelial surface. **d**, **e**, Greyscale-inverted images from **a** showing conservation of cell contacts throughout cell division. **d**, Dilation of the junctional lattice permits rounding of a seven-sided mitotic cell during stages corresponding to prophase–metaphase. Owing to compression and stretching of the pseudo-coloured neighbours, no cell–neighbour exchanges occur ($n = 18$ dilating cells). Units of t are in minutes. **e**, During stages corresponding to anaphase through cytokinesis, local topology (connectivity between cells) remains unchanged; the mitotic cell approaches abscission surrounded by the same cohort of seven neighbours ($n = 23$ cytokinetic cells). **f**, Two-cell clones marked by heritable expression of GFP (green) imaged at the level of the septate junctions stained with anti-Dlg (red). **g**, In approximately 94% of cell divisions, cytokinesis resolves with formation of a new cell interface, resulting in the type I conformation of mitotic siblings. **h**, Summary diagram of topology changes during cell division.

division. This behaviour is independent of cleavage plane orientation, and is instead a result of the formation of tricellular junctions, as previously demonstrated for plant tissues^{7–9}. Importantly, however, an average of six does not necessitate a prevalence (or even existence) of hexagons and so a higher fidelity model is required.

We formulated a more precise model using a discrete Markov chain to capture the stochastic nature of cell proliferation, inspired by mathematical work on random space-dividing topologies²³. We defined the state of a cell, s , as its number of sides where $s > 3$. The relative frequency of s -sided cells in the population was defined as p_s , and the state of the population at generation t as an infinite row vector $\mathbf{p}^{(t)} = [p_4 p_5 p_6 p_7 p_8 p_9 \dots]$. The state dynamics is described by $\mathbf{p}^{(t+1)} = \mathbf{p}^{(t)}PS$, where P and S are probabilistic transition matrices (Box 1). Briefly, the entries P_{ij} represent the probability that an i -sided cell will become j -sided after mitosis. Topological arguments indicate that a cell will gain an average of one new side per cycle due to neighbour divisions, and the matrix S accounts for this effect. Thus, given the distribution of polygonal cell types $\mathbf{p}^{(t)}$, we can compute the new distribution after a single round of division.

Formulating epithelial topology as a Markov chain (Fig. 2a) yields a strong quantitative prediction: that a stable equilibrium distribution of polygons should emerge in proliferating epithelia, irrespective of the

Box 1 | Derivation of Markov state dynamics

Here we derive the probabilistic transition matrices P and S . The entry P_{ij} is the probability that an i -sided cell divides to produce a j -sided daughter cell. Consider a single cell with s_{t-1} sides (or junctions) at generation $t - 1$. Let the random variable K_t represent the number of junctions distributed to one daughter cell on division at generation t , leaving $s_{t-1} - K_t$ for the other. Because no triangular cells are observed empirically, we assume that each daughter receives at least two junctions from the parent, leaving $s_{t-1} - 4$ junctions to be distributed among the daughters. Assuming that junctions are distributed uniformly at random around the mitotic cell and that cleavage plane orientation is chosen uniformly at random (to bisect the rounded mitotic cell's area), we can model the distribution of these remaining junctions as balls thrown into one of two bins (daughters) with equal probability. Thus, the number of additional parental junctions received by the first daughter is $K_t - 2$, a binomial random variable with parameters $n = s_{t-1} - 4$, $p = \frac{1}{2}$. Finally, each daughter also gains two new junctions as a result of the newly created interface. Therefore, the probability of transition from an i -sided cell to a j -sided daughter is $P_{ij} = \Pr[K_t + 2 = j | s_{t-1} = i] = \text{Comb}(i - 4, j - 4) / 2^{i-4}$, where $\text{Comb}(a, b)$ is the number of ways to choose b objects from a set of a objects. As a consequence, the (un-normalized) entries of P are the coefficients of Pascal's triangle.

Next we derive the 'shift matrix' S , the entries, S_{ij} , of which represent the probability that an i -sided cell will gain sides from dividing neighbours to become j -sided. Thus, S accounts for the effect of neighbour cell divisions on the polygon class of a given cell, an effect that was unaccounted for in previous work²³. On mitosis, a cell adds one side to each of two neighbouring cells. Assuming N cells in an epithelium, this means that $+2N$ sides are added during one round of divisions, resulting in $2N$ cells. Hence, the average number of sides gained per cell is $+2N/2N = +1$. That is, a cell will gain, on average, one side per cycle from dividing neighbours. Thus, the entries of the matrix S are $S_{ij} = 1$ if $j = i + 1$ and zero otherwise. Note that this is a mean-field approximation of the effect of dividing neighbour cells. In reality, some cells will gain no sides and others will gain more than one side.

P		Post-mitotic class							S		After neighbour divisions						
		4	5	6	7	8	9	10			4	5	6	7	8	9	10
Pre-mitotic class	4	1							Before neighbour divisions	4	0	1					
	5	1	1							5		0	1				
	6	1	2	1						6			0	1			
	7	1	3	3	1					7				0	1		
	8	1	4	6	4	1				8					0	1	
	9	1	5	10	10	5	1			9						0	1
	10							...		10							...

initial conditions (Perron–Frobenius theorem)²⁴. We calculated the exact equilibrium E directly from the matrix $T = PS$ to be approximately 28.9% pentagons, 46.4% hexagons, 20.8% heptagons and lesser frequencies of other polygon types (Fig. 2b; see Methods). The model also predicts that the population of cells should approach this distribution at an exponential rate. Consequently, global topology converges to E in less than eight generations, even for initial conditions where every cell is quadrilateral, hexagonal, or nonagonal (Fig. 2c). Furthermore, we modelled defective interface formation between mitotic siblings, and found that E is robust to small error rates (Supplementary Data).

To validate whether E exists *in vivo*, we determined the actual polygon distribution in the developing *Drosophila* wing. Notably, empirical counts closely matched E for every major polygon class to within a few per cent ($n = 2,172$ cells; Fig. 3a). Only the small percentage of four-sided cells was unaccounted for, an effect attributable to the mean field approximation (Box 1 and Supplementary Data). In addition, the variation between individual imaginal discs was minimal (see error bars for Fig. 3a; see also Supplementary Fig. 2). Our first-order Markov model can therefore explain global topology in the *Drosophila* wing disc epithelium, including the predominance of hexagons, based on the mechanism of cell division alone. A unique advantage of this simple model is its generality, particularly given the conservation of fundamental aspects of adhesion and mitosis in monolayer epithelia. Consistent with this, we found that polygon topology in the tadpole tail epidermis of the frog *Xenopus* ($n = 1,051$ cells) and in the outer epidermis of the freshwater cnidarian *Hydra* ($n = 602$ cells) also closely approached E (Fig. 3a). Although the details of cell division in these organisms remain to be described, we infer that the same equilibrium topology will emerge in most multicellular eukaryotes. Indeed, the reported cell topology in plant epidermis is in remarkably close agreement with our results (25.1% pentagons, 47.4% hexagons and 22.4% heptagons)⁸.

In addition to predicting the equilibrium topology, our model also

provides a quantitative framework for further insights into epithelial organization. For example, the model predicts that each cell in the population must gain an average of one side per cell cycle (Box 1). Confirming this, we found that the average mitotic cell (at the end of the cell cycle) possessed not six (5.94 ± 0.06) but rather seven sides (6.99 ± 0.07 ; Fig. 3b, c; $n = 177$ mitotic figures). This indicates that epithelial cells accumulate additional sides until mitosis, at which time they divide into two daughters of lesser sidedness. Topological equilibrium is therefore achieved as a balance between autonomous and non-autonomous division events.

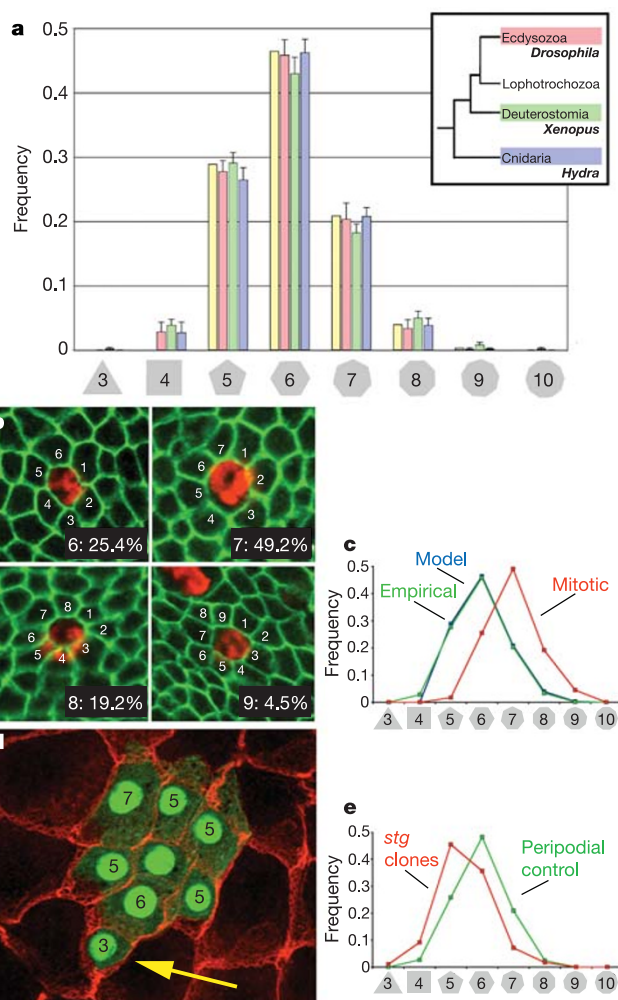


Figure 3 | An emergent topological order in proliferating epithelia. **a**, In close accordance with the theoretical equilibrium topology (yellow), *Drosophila* wing disc (pink, $n = 2,172$ cells), *Xenopus* tail epidermis (green, $n = 1,051$ cells) and *Hydra* epidermis (blue, $n = 602$ cells) all exhibit a similar non-gaussian distribution of epithelial polygons with less than 50% hexagonal cells and high (and asymmetric) percentages of pentagonal and heptagonal cells. Error bars indicate standard deviation between individual samples. The inset indicates relative phylogenetic positions for *Drosophila*, *Xenopus* and *Hydra*²⁶. **b**, Prophase cells (marked with anti-phospho-histone H3; red) stained for cell junctions (Dlg, green) to quantify cell sidedness. Most mitotic cells are seven-sided. **c**, Polygonal cells in the Markov model (predicted, blue) and *Drosophila* wing disc (empirical, green) have an average of six sides. The population of mitotic cells is shifted, reflecting an average of seven sides. **d**, Cells on the periphery of a *string*-expressing clone (green) in the peripodial epithelium have fewer sides. Note the presence of a triangular cell, not observed under normal circumstances (yellow arrow; Dlg, red). **e**, The distribution of polygon types on the periphery of *string*-expressing clones (red; $n = 295$ cells in 24 clones) is shifted to reflect a predominance of pentagons, and deviates from controls (green, $n = 411$ wild-type peripodial cells).

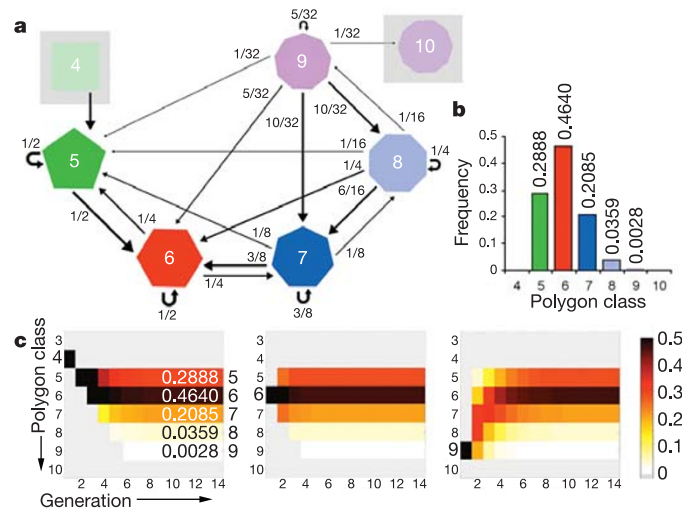


Figure 2 | A robust equilibrium topology in proliferating epithelial cell networks. **a**, Schematized Markov chain model representing proliferation dynamics for polygonal cells. Cells occupy a series of discrete states representing polygon classes from four to nine sides. To simulate a round of division, cells either recycle to the same state (curved arrows) or transition to a new state (straight arrows) according to the probabilities encoded by the neighbour effect transition matrix T (expressed here as fractions). Transitions from states s with an equilibrium probability $p_s < 10^{-4}$ have been omitted for clarity. **b**, Within ten generations, the distribution of polygonal shapes converges to E , comprising 28.88% pentagons, 46.40% hexagons, 20.85% heptagons, 3.59% octagons and 0.28% nonagons. **c**, Emergence of E regardless of initial conditions where all cells are uniformly quadrilateral, hexagonal or nonagonal.

One consequence of this result is that localized deviations in the rate of cell proliferation should predictably distort local topology. To test this, we took advantage of the fact that peripodial cells of the wing disc maintain the distribution *E*, but cease dividing by the mid-third larval instar. By misexpressing the mitosis-promoting phosphatase *string*²⁵ we drove peripodial cell clones through extra divisions, creating sharp boundaries between over-proliferating cells and their quiescent neighbours (Fig. 3d). Consistent with our model, dividing cells bounded by quiescent cells had fewer sides than controls (an average of 5.42 ± 0.14 sides compared with 5.94 ± 0.15 , respectively; Fig. 3e). In fact, three of 24 *string*-expressing peripodial clones contained triangular cells (Fig. 3d, yellow arrow), which were not observed in wild-type cells. These results demonstrate an unforeseen mechanism by which differential proliferation could influence cell shape and morphogenesis, or alternatively, cause the dysplastic tissue architecture observed in various forms of proliferative disease.

We propose that the division mechanism of adherent epithelial cells is not only mathematically sufficient to explain the predominantly hexagonal topology of epithelia, but also to predict the overall distribution of polygonal cell types. As a result, epithelial topology is irregular, but not random. Our results indicate that a simple emergent mechanism determines cell shape, suggesting a means by which epithelia accommodate rapid proliferation while maintaining uniform structural integrity. Looking forward, the Markov model formulation provides a new framework for investigating other models of cell division, such as different cleavage plane choices or aberrant cell division. This may be of general utility in understanding how stochastic behaviour at the single cell level manifests in global patterns in a multicellular context.

METHODS

Confocal time lapse. We used standard Ringer's solution (130 mM NaCl, 5 mM KCl, 1.5 mM MgCl₂) as well as Shields and Sang M3 insect media (Sigma-Aldrich; modified with 10% fetal bovine serum, 10 mU l⁻¹ insulin, 10 U ml⁻¹ penicillin, 10 µg ml⁻¹ streptomycin) to obtain movies over culture periods of 1.5–2 h at maximum.

Clonal analysis and imaging. GFP-expressing clones were induced in flies of the genotype: *yw hs-flp*¹²²; *Actin5c* >> *Gal4*, *UAS-GFP/+* with a 15-min heat shock at 37°C followed by a 10-h recovery period. *string*-expressing clones were induced in the same genotype with *UAS-sg* (Bloomington Stock Center) crossed onto chromosome III. For immunocytochemistry and phalloidin staining, *Drosophila* imaginal discs, whole *Hydra* and *Xenopus* tail epidermis were fixed in 4% paraformaldehyde in PBS. Images were collected on a Leica TCS SP2 AOBS confocal microscope system and processed using Adobe Photoshop 7.0 software.

Polygon distributions. Polygon distributions were determined by eye in confocal micrographs; error was estimated as the average standard deviation between counts from different images. Empirically, it was not possible to account systematically for certain rare but inevitable irregularities in real epithelia, such as occasional four-way point junctions and dying or grossly misshapen cells. The raw counts for cells of different sidedness are as follows: *Drosophila* disc columnar epithelium (4, 64; 5, 606; 6, 993; 7, 437; 8, 69; 9, 3). *Hydra* (4, 16; 5, 159; 6, 278; 7, 125; 8, 23; 9, 1). *Xenopus* (3, 2; 4, 40; 5, 305; 6, 451; 7, 191; 8, 52; 9, 8; 10, 2). *Drosophila* peripodial controls (4, 11; 5, 106; 6, 198; 7, 86; 8, 10; 9, 0). *Drosophila* peripodial *string* clones (only cells on the clone periphery were scored: 3, 3; 4, 27; 5, 134; 6, 105; 7, 21; 8, 5; 9, 0).

Markov chain convergence and equilibrium distribution calculation. The Perron–Frobenius theorem²⁴ guarantees that an irreducible and aperiodic Markov chain will converge to a unique stable equilibrium **p**^{*}, where **p**^{*} is the principal eigenvector of the transition matrix *T*. We truncated the infinite transition matrix *T* down to 20 rows and 20 columns and then used Matlab to calculate **p**^{*}. We also computed λ₂, the second-largest eigenvalue of *T*, as 0.5, which determines the rate of convergence.

Received 13 March; accepted 23 June 2006.

Published online 9 August 2006.

1. Schwann, T. *Microscopical Researches into the Accordance of Structure and Growth in Animals and Plants* (Syndenham Society, London, 1847).

2. Thompson, D. W. *On Growth and Form* (Cambridge Univ. Press, Cambridge, 1942).
3. Hayashi, T. & Carthew, R. W. Surface mechanics mediate pattern formation in the developing retina. *Nature* **431**, 647–652 (2004).
4. Amonlirdviman, K. et al. Mathematical modeling of planar cell polarity to understand domineering nonautonomy. *Science* **307**, 423–426 (2005).
5. Weaire, D. & Rivier, N. Soap, cells and statistics—Random patterns in two dimensions. *Contemp. Phys.* **25**, 59–99 (1984).
6. Abbott, L. A. & Lindenmayer, A. Models for growth of clones in hexagonal cell arrangements: Applications in *Drosophila* wing disc epithelia and plant epidermal tissues. *J. Theor. Biol.* **90**, 495–544 (1981).
7. Lewis, F. T. The effect of cell division on the shape and size of hexagonal cells. *Anat. Rec.* **33**, 331–355 (1926).
8. Lewis, F. T. The correlation between cell division and the shapes and sizes of prismatic cells in the epidermis of *Cucumis*. *Anat. Rec.* **38**, 341–376 (1928).
9. Graustein, W. C. On the average number of sides of polygons of a net. *Ann. Math.* **32**, 149–153 (1931).
10. Garcia-Bellido, A. & Merriam, J. R. Parameters of the wing imaginal disc development in *Drosophila melanogaster*. *Dev. Biol.* **24**, 61–87 (1971).
11. Bryant, P. J. & Levinson, P. Intrinsic growth control in the imaginal primordia of *Drosophila*, and the autonomous action of a lethal mutation causing overgrowth. *Dev. Biol.* **107**, 355–363 (1985).
12. Milan, M., Campuzano, S. & Garcia-Bellido, A. Cell cycling and patterned cell proliferation in the wing primordium of *Drosophila*. *Proc. Natl Acad. Sci. USA* **93**, 640–645 (1996).
13. Tepass, U., Tanentzapf, G., Ward, R. & Fehon, R. Epithelial cell polarity and cell junctions in *Drosophila*. *Annu. Rev. Genet.* **35**, 747–784 (2001).
14. Bertet, C., Sulak, L. & Lecuit, T. Myosin-dependent junction remodelling controls planar cell intercalation and axis elongation. *Nature* **429**, 667–671 (2004).
15. Zallen, J. A. & Zallen, R. Cell-pattern disordering during convergent extension in *Drosophila*. *J. Phys. Condens. Matter* **16**, S5073–S5080 (2004).
16. Classen, A. K., Anderson, K. I., Marois, E. & Eaton, S. Hexagonal packing of *Drosophila* wing epithelial cells by the planar cell polarity pathway. *Dev. Cell* **9**, 805–817 (2005).
17. Morin, X., Daneman, R., Zavortink, M. & Chia, W. A protein trap strategy to detect GFP-tagged proteins expressed from their endogenous loci in *Drosophila*. *Proc. Natl Acad. Sci. USA* **98**, 15050–15055 (2001).
18. Kelson, R. J. et al. Flytrap, a database documenting a GFP protein-trap insertion screen in *Drosophila melanogaster*. *Nucleic Acids Res.* **32**, D418–D420 (2004).
19. Bryant, P. J. Cell lineage relationships in the imaginal wing disc of *Drosophila melanogaster*. *Dev. Biol.* **22**, 389–411 (1970).
20. Garcia-Bellido, A., Ripoll, P. & Morata, G. Developmental compartmentalisation of the wing disk of *Drosophila*. *Nat. New Biol.* **24**, 251–253 (1973).
21. Resino, J., Salama-Cohen, P. & Garcia-Bellido, A. Determining the role of patterned cell proliferation in the shape and size of the *Drosophila* wing. *Proc. Natl Acad. Sci. USA* **99**, 7502–7507 (2002).
22. Struhl, G. & Basler, K. Organizing activity of wingless protein in *Drosophila*. *Cell* **72**, 527–540 (1993).
23. Cowan, R. & Morris, V. B. Division rules for polygonal cells. *J. Theor. Biol.* **131**, 33–42 (1988).
24. Taylor, H. M. & Karlin, S. *An Introduction to Stochastic Modeling* 3rd edn (Academic, Chestnut Hill, Massachusetts, 1998).
25. Edgar, B. A. & O'Farrell, P. H. The three postblastoderm cell cycles of *Drosophila* embryogenesis are regulated in G2 by *string*. *Cell* **62**, 469–480 (1990).
26. Halanych, K. M. & Passamaneck, Y. A brief review of metazoan phylogeny and future prospects in Hox-research. *Am. Zool.* **41**, 629–639 (2001).

Supplementary Information is linked to the online version of the paper at www.nature.com/nature.

Acknowledgements We thank R. Ward, J. D. Lambert, B. Mathey-Prevot, E. Lieberman, R. Arnaout and M. Markstein for critical comments on the manuscript; the Bloomington Stock Center for fly stocks; and the Developmental Studies Hybridoma Bank for antibodies. This work was supported by a Microscopy New Faculty Fellowship to R.N., an NSF grant to R.N., and support from the Howard Hughes Medical Institute to N.P. A.B.P. is a fellow of the National Science Foundation and M.C.G. was supported by the Jane Coffin Childs Memorial Fund for Medical Research.

Author Contributions R.N. and N.P. are senior authors. A.B.P. and M.C.G. contributed equally to the work.

Author Information Reprints and permissions information is available at www.nature.com/reprints. The authors declare no competing financial interests. Correspondence and requests for materials should be addressed to M.C.G. (mgx@stowers-institute.org) or R.N. (rad@eecs.harvard.edu).